2018 Building Performance Analysis Conference and
SimBuild co-organized by ASHRAE and IBPSA-USA
Chicago, IL
September 26-28, 2018

AN EXPERIMENTAL AND NUMERICAL MODEL OF A SOLAR FACADE PROTOTYPE WITH TRANSPARENT INSULATION AND SELECTIVE ABSORBER

Miroslav Čekon[1], Josef Plášek[1], Richard Slávik[1], Tomáš Fečer[1] and Peter Juráš[2]
[1]Centre AdMaS, Brno University of Technology, Brno, Czechia
[2]Faculty of Civil Engineering, University of Žilina, Žilina, Slovakia

ABSTRACT

The presented study focuses on the modelling of a Transparent Insulation Material (TIM) incorporated in a façade structure. An experimental prototype of a Transparent Insulation Façade (TIF) with and without a selective absorber was developed as part of the opaque building envelope. Experimental measurements were performed using a climatic chamber test with the aim of verifying theoretical models. A detailed comparative investigation of the thermal performance of both TIFs was conducted using numerical CFD methods. The proper consistency between the simulation results and the experimental data indicated that the simulation model was reliable for predicting the overall thermal performance of TIM based solar façade prototypes.

INTRODUCTION

The improved thermal insulation offered by integrating transparent insulation material (TIM) into building façades can ultimately affect the overall energy efficiency of the building. Different studies in the last two decades developed the solar walls with TIMs replacing the original glazing elements. Hence, the development of various innovative concepts of building envelopes, and their practical implementation, can be enhanced by applying the proper performance prediction theoretical models. Experimental tests in conjunction with numerical computations may validate and improve performance prediction models of building envelopes, such as novel solar thermal façade elements. This area needs to be studied to accurately predict the thermal and energy performance in the context of applying TIMs on a solar façade concept.

Current building energy simulation tools are not accurate enough for modelling these complex transparent insulation systems, often because of the simplified thermal and optical models used to solve heat transfer as well as light transmittance. Basically, one dimensional methods are used for both thermal transfer and solar transmittance through these systems (Sun et al. 2018). In practice, with the integration of a more complex structure within the air cavity of a double glazing unit, there will be a significant effect on the free convection, long-wave radiative heat transfer and solar energy transmitted through the system that have not been typically considered. This was recently analyzed by Sun (2017) to comprehensively study all those aspects in glazing system with TIM for building energy saving and daylight comfort. They aimed to develop a comprehensive method to analyse these specific glazing systems (Sun et al. 2017). Specifically, in most of the previously conducted studies, long-wave radiation heat transfer, which accounts for two thirds of the total heat transfer across the air cavity (Gan 2001), is neglected within TIM-based structure during numerical modelling. In addition, when integrated in a building opaque element with multilayer structure that employ several low-e functionalities, this can result in a completely different situation and and give rise to a more complex task that needs to be considered.

Although, the thermal resistance of the glazing system varies with the change of the mean temperature of the glazing and the temperature difference between the two glazing panes, detailed investigations of the interstitial structure on the reduction of heat transfer in terms of both convection, which is driven predominately by temperature difference across the two glass panes, and radiation, which is driven predominately by glazing system mean temperature, under different environmental conditions that are commonly encountered in buildings are less well studied (Sun et al. 2016). The improved simulation methods have been implemented by Avedissian and Naylor (2008), who used a surface-to-surface model to include radiation, however they only used the model to calculate the *U*-value of the whole system instead of evaluating the effects of the internal structure on long-wave radiative heat transfer.

Brandl et al. (2015) developed a three-dimensional (3D) Computational Fluid Dynamics (CFD) model for the analysis of the thermal behaviour of a solar honeycomb (SHC) façade element using the cellulose honeycomb TIM in steady state conditions. Laboratory experiments were performed and the measured data were used for the validation of the 3D CFD models of the SHC element. Moreover, the impact of the SHC's material properties on the dynamic thermal behaviour was analysed with this CFD model. This was primarily focused on further

comprehensive analysis of the transient thermal behaviour of a SHC façade element with and without integrated photovoltaic (PV) cells (Brandl et al. 2016).

The aim of this study is to focus on standard calculation and a Computational Fluid Dynamics (CFD) numerical analysis of the transparent insulation façade (TIF) prototype using Polymethylmethacrylate (PMMA) honeycomb TIM integrated in a particular glazing system and its validation. A solar façade prototype based on TIM glazing system coupled with a selective absorber (SA) is developed and compared with a non-selective absorber (nSA) type, respectively. The objective of this analysis is to identify the thermally effective parameters for building integrated TIF and two solar absorber concepts with different emissivity. To comprehensively investigate the thermal characteristics of a PMMA honeycomb TIF in the opaque part of the façade and predict the thermal performance of the building when the specific TIM glazing system is incorporated, a numerical 3D CFD model has been developed. This has been used to investigate the thermal resistance across the whole TIF prototype involving the variation of environmental conditions (varying temperature conditions). This was primarily focused on the comparability between both real and modelled outputs. In the first part, model validation for appropriate modelling and simulation of a given solar based prototype is demonstrated. In the second part, the capability of real and modelled performance is analysed, in terms of its ability to theoretically describe thermal performance of the presented solar façade model.

METHODOLOGICAL APPROACH

An experimental investigation is conducted in a large climatic chamber, and the measurement results were used to validate a standard calculation and 3D CFD models. Various boundary temperature conditions were applied during the measurements, excluding wind and solar radiation effects. Combined with the measured thermal properties of the facade prototype, a standard calculation and an integrated model were developed to simulate the thermal performance of the TIM based solar facade prototype with and without a selective absorber.

Through this approach, the thermal characterisations of two TIFs can be comprehensively obtained from the CFD simulation. All of this information will be expected to provide a thermal characterisation of a TIF system into building energy simulation models to obtain building heating and cooling energy loads, when honeycomb TIM is integrated within the opaque façade structure.

EXPERIMENTAL MEASUREMENT

Experimental measurements of the analysed TIF prototypes were carried out at the Research Centre of the University of Žilina (Slovakia). Two prototypes with (SA) and without a selective absorber (nSA) were compared under a series of temperature-controlled conditions. The experimental apparatus, the measured prototypes and the measurement procedure are described in following section.

The climatic chamber

The climatic chamber (Figure 1) provides a steady and cyclical simulation of the climatic environment consisting of two chambers: chamber for simulation of outdoor climate has dimensions of 2 m x 1.8 m x 1.5 m and a volume of 7.2 m^3, the indoor chamber has a volume of 6.6 m^3. The maximum dimension of the measured sample can be 2 m x 1.8 m. For the purpose of this measurement, a masking panel with an aperture of 1.23 m x 1.48 m was used. During the test, the integral air conditioning units can be used to control the temperature of the two chambers within the range of -40 to +80°C and the relative humidity between 10 and 95%. Various parameters such as surface temperature, air temperature and heat flux of the test sample, can be obtained during operation. An experimental test implementing TIF prototypes (Figure 1 and 2) was prepared, using the TIM system with two solar absorbers and tested in the climatic chamber under different boundary conditions.

Figure 1 Climatic chamber used and integrated TIF prototype prepared for measurement

Test samples and apparatus setup

A transparent insulation façade (TIF) concept was designed to analyze the emissivity changing within air cavity layer behind the transparent insulation system. This model incorporates a gypsum board (GB) of 25 mm thickness as the base layer for integration of solar absorber. Two 1.19 m x 1.19 m test prototypes (Figure 2) were built using a system based on the Kapilux

transparent insulation system that implements honeycomb transparent PMMA based insulation. Each was equiped with a different type integrated solar absorber (SA and nSA). The used materials and geometrical parameters are shown in Figure 3.

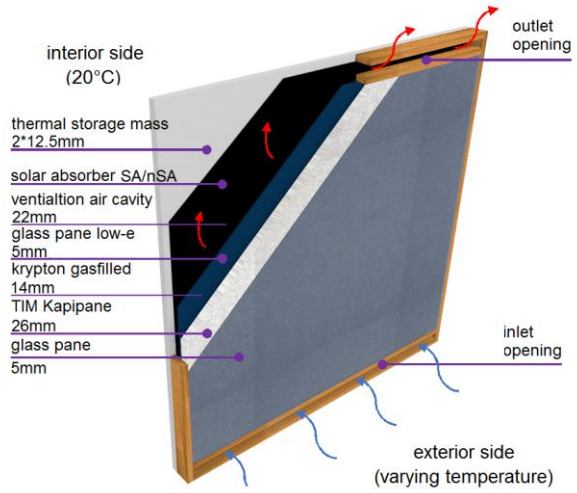

Figure 2 TIF model and material layers

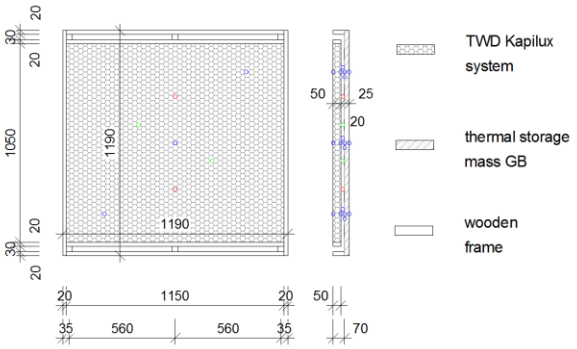

Figure 3 Basic materials and geometrical parameters

The declared thermal and optical properties of the TIM system are as follows: thermal transmittance U_{TIM} is 0.7 W/(m^2 K), total solar energy transmittance or solar heat gain coefficient is 61% and light transmission represents 70%. Basically, the TIF concept consists of several functional layers. Firstly, it represents the thermal and transparent insulation functionality on TIM basis, coupled with non-ventilated krypton gas-filled cavity using a specific commercially available glazing unit system. Secondly, it applies an additional air cavity. Thirdly, it is based on two types of absorber, selective SA and non-selective nSA type. The last material is the base layer for application of solar absorber. In real façade this would also fulfil the role of heat accumulation layer. For the purpose of the described experiment this layer is simplified to a 25mm gypsum board (GB) panel. This is intended for it to provide a performance prediction model of TIM system coupled with the two different solar absorbers. Hence, the main difference between both prototypes was in their absorbing part. Both have almost the same solar absorbance at the level of around 0.94 and 0.96, while their emissivity has a completely opposite level of 0.06 (SA) and 0.94 (nSA), respectively.

Six measuring positions along the test sample were measured, each interface on the diagonal line consisting of three sensors (Figure 4): the air temperature in the air cavity (*ai*), the surface absorber temperature (*si_abs*), the internal surface temperature of TIM system (*si_TIM*), the material interface between the absorber and the GB layer (*nSA/SA*) and the internal surface temperature (*si*) of TIF prototypes. Temperatures were measured using the Pt100 sensors (Type CRZ 2005-100, class A, tolerance 0.15+0.002t). Heat flux was measured by a circular cross section heat flux plates AHLBORN FQA020C with a diameter of 33 mm. Velocity in the air cavity was measured with AHLBORN FVAD35TH4 at a resolution of 0.01 m/s and an accuracy of 0.05 m/s.

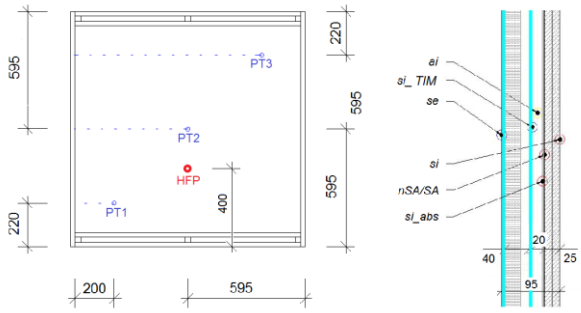

Figure 4 Sensors´ positioning Pt100, heat flow plates HFP and profile of measured temperatures

Measurement procedure and obtained data

For the purpose of these tests, only different temperature conditions were tested. The four test conditions maintained the air temperatures in both chambers (θ_i and θ_e) represent four test scenarios. All scenarios aimed at keeping the internal air temperature of the interior chamber at a constant temperature of 20°C; however, varying the air temperature in exterior cold chamber from -20 to +10°C. This means that four temperature gradients from 10 to 40°K were experimentally monitored. Because the only difference between the two tested prototypes is the emissivity changing on the solar absorber side, their influence on thermal resistance can be directly evaluated. Generally, tests were conducted for a sufficient duration (each case over 7 h) to allow the environmental conditions in the test rooms and the heat

flow through the measured sample to stabilize for each test case, and then the data measured over a further period of 3 h were used for the analysis. The measurement method followed the standard practice for *in situ* thermal resistance measurements using heat flow meters. The sample's surface temperature (θ_{si} and θ_{se}) and heat flux ($\bar{q}$) were measured or calculated during the experimental test and an average method was used to analyse the data and obtain the thermal resistance (R) of the developed prototypes by using Eq. (1):

$$R = \frac{(\theta_{si} - \theta_{se})}{\bar{q}} \quad (2)$$

Two heat fluxes were measured by heat flux plates and the values were subsequently corrected according to the datasheet specification of temperature dependency. Third heat flux was calculated from U value of TIM system and the temperature gradient of its surfaces. The last heat flux was obtained with the known thermal conductivity of gypsum board layer, its thickness and temperature gradient. Each heat flux uses the last 10-15 min of each temperature regime, when the temperature profile reaches steady state. Finally, the sample heat flux ($\bar{q}$) was obtained as an average of these four heat fluxes.

THEORETICAL ANALYSIS

This section presents key aspects of the theoretical calculations employed to predict the performance of the presented TIF prototypes with and without a selective absorber.

Standard calculation

Generally, the simplified procedure for the thermal performance evalaution of experimental measurements on measured samples is to compare the measured results with the results obtained using the standard calculation method. The TIM glazing unit and base GB layer were used with known equivalent thermal characteristics as solid volumes. Thus, their both thermal resistances were directly used for standard calculation of both elements. As the key variable that affect the overall thermal perfomance of both TIF prototypes is the determination of the thermal resistance of their airspace R_g between TIM and GB layer with solar absorber plate, the empirical equations given in ISO 6946 (2007) need to be employed. The thermal resistance between these solid surfaces consists of the radiative heat transfer (h_r) and the heat transmittance through the air by convection and conduction (h_a) (2).

$$R_g = \frac{1}{h_a + h_r} \quad (2)$$

The conduction/convection coefficient for closed vertical cavities and temperature difference less than 5 K is calculated in a simplified manner: h_a is the maximum between 1.250 $W.m^{-2}.K^{-1}$ and the quantity 0.025 divided by the air space depth. Thus, the wider air spaces than 0.02 m have no influence on calculation heat transfer. When the temperature difference across the airspace exceeds 5 K, convective heat transfer is calculated in a temperature gradient effect (3):

$$h_a = 0.73 \times \Delta T^{1/3} \quad (3)$$

As for the radiation coefficient (h_r), the thermodynamic temperature gradient of the surfaces and their emissivity values (ε_1 and ε_2) participating in radiation heat exchange based on (4) are employed.

$$h_r = \frac{1}{\left(\frac{1}{\varepsilon_1} + \frac{1}{\varepsilon_2} - 1\right)} \times \frac{\left({T_1}^4 - {T_2}^4\right)}{(\theta_1 - \theta_2)} \times 5.67.10^{-8} \quad (4)$$

CFD simulation

The main parameters of the numerical CFD simulation employed to reproduce the experimental measurement are described in this section. The thermal performance of a transparent insulation façade (TIF) with a selective and non-selective absorber were investigated at four different temperature gradients varying only the temperature on external surface. The numerical CFD simulation was conducted in the software ANSYS version 17.2. This double parametric CFD numerical simulation was performed a variable emissivity of the absorber for a constant value ε = 0.06 (SA) and ε = 0.94 (nSA). The calculation geometry of TIF model was created in software ANSYS Modeller by solid volume of wooden frame (WF), solid volume of gypsum board (GB), fluid volume of unvented airspace and solid volume of double glazing unit with TIM. In this study, the double glass unit with TIM was simplified on solid volume with equivalent thermal characteristics. This calculation geometry of the TIF model was discretized by hexahedral, prismatic and pyramidal shapes with the count of 164 306 elements in ANSYS Meshing software (see Figure 5). The minimum orthogonality quality of the calculation grid was obtained at 0.213, maximum orthogonally skew was obtained at 0.735 and maximum aspect ratio was obtained at 1.653.

The calculation grid was imported to software ANSYS Fluent version 17.2. This model was extended on operating condition with natural gravity -9.81 m/s² on the Y axis and, consequently, the material characteristics were defined for each volume in the calculation grid. The internal boundary condition was assigned as a constant surface temperature at +20°C and the external surface

temperature was changed in the range of -20 to +10°C at 10°C step. The peripheral surface of the wooden frame was calculated as temperature symmetry (adiabatic wall). The numerical model of TIF was initialized by automatic standard method at constant values.

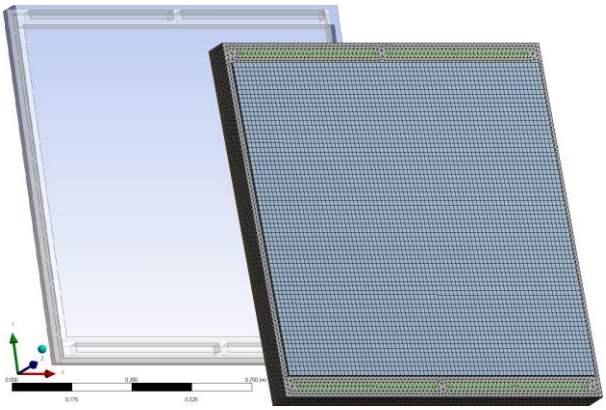

Figure 5 Geometry and calculation grid of TIF model in software ANSYS Fluent version 17.2.

The parametrical CFD numerical simulation in software ANSYS Fluent 17.2 was parametrized on pressure-base with heat transfer driven by energy equation, radiation model discrete ordinates (DO) and mass transfer driven by Reynolds stress viscous model (7 equations) with Buoyant effect. The solution method was applied as a second order against the wind for the energy equation, pressure balance, airflow momentum, turbulent kinetic energy and turbulent dissipation rate. The convergence criterion was assigned to a residual value of less than 10^{-6} in energy equation, as well as for continuity and air velocities. The count of iteration steps was greater than the 10^5 iteration for each parametric case..

RESULTS AND DISCUSSION

The results from the experimental measurement are presented in this section and compared with the standard calculation, as well as with numerical CFD simulation. A detailed analysis through the CFD simulation of the TIF prototypes with and without a selective absorber were compared with the measured results to validate the accuracy of numerical modelling. The data obtained by standard calculation method and parametric numerical CFD simulation are finally used for approximation of a convective heat transfer relation to improve consistency between standard calculation model and measurement.

Experimental measurement

The data of air temperatures; surface temperatures and heat fluxes were measured, and the calculated thermal resistances in four temperature gradients corresponding to four boundary conditions are shown in Table 1. The data presented show the results indicating a difference in the thermal performance of the SA sample compared to the reference nSA sample. Based on the measured results, the nSA concept showed an almost constant thermal resistance between 1.20 and 1.24 (m^2·K)/W, while the SA concept displayed a maximum of 1.73 (m^2·K)/W at 10K temperature (the difference between the indoor and outdoor chamber), while with its increase of up to 40K, the thermal resistance significantly decreases at the level of 1.55 (m^2·K)/W. This means, depending on temperature conditions, that the emissivity changing of the solar absorber inside the unvented air space can increase the thermal properties of the nSA type from 21 to 29%.

Table 1 Measured thermal resistance

Temperature difference (K)	Measured thermal resistance R_{mes} (m^2·K)/W	
	SA	nSA
10	1.73	1.22
20	1.67	1.23
30	1.62	1.24
40	1.55	1.23

Calculation results

The calculated data of thermal resistance using the standard method according to ISO (2007) are presented in Table 2. Using the calculation of both convection/conduction and radiation coefficients according to standard method, the effect of the thermal resistance on the temperature difference is evident with emissivity changing, however only with low-e functionality of solar absorber. Based on the calculated values, the nSA concept showed an almost constant thermal resistance between 1.31 and 1.33 (m^2·K)/W, while the SA concept displayed a maximum of 1.76 (m^2·K)/W at 10K temperature, while with its increase of up to 40K, the thermal resistance decreases at the level of 1.64 (m^2·K)/W. This means, that the unvented airspace with standard calculation increases the thermal properties of the nSA type from 19 to 26%.

Table 2 Calculated thermal resistance

Temperature difference (K)	Calculated thermal resistance R_{calc} (m^2·K)/W	
	SA	nSA
10	1.76	1.31
20	1.73	1.32
30	1.68	1.33
40	1.64	1.33

Numerical simulation

As above introduced simulation parameters, the results in this section are demonstrated in detail using parametric numerical CFD simulation in software ANSYS Fluent version 17.2. The obtained surface temperature of both SA/nSA prototypes is compared in Table 3 and a chosen state from parametric numerical CFD simulation is plotted as illustrated in Figure 6 for particular temperature gradient -10°C/ +20°C.

Overall, the temperature difference between the real measured temperature in the climatic chamber and the results obtained from parametric numerical CFD simulation are lower than ±0.40°C (see Table 3).

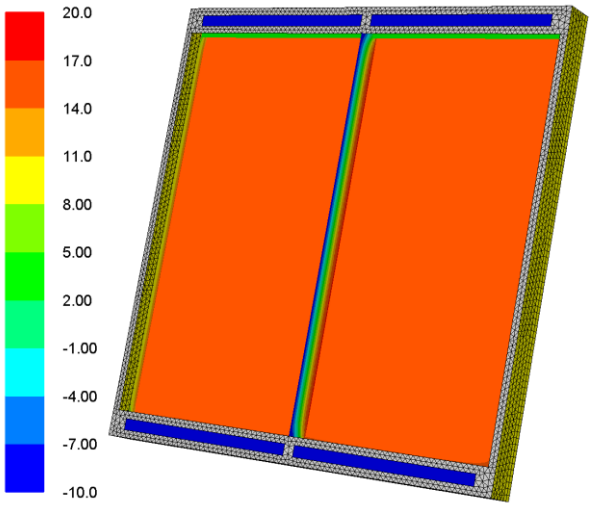

Figure 6 - Surface temperature of selective absorber for temperature gradient -10°C / +20°C.

Table 3 Comparison of absorber temperature

Temperature Gradient	Method	SA	nSA
-20°C / 20°C	Measurement	13.1°C	-2.7°C
	Simulation	13.5°C	-2.6°C
-10°C / 20°C	Measurement	15.4°C	3.0°C
	Simulation	15.7°C	3.1°C
0°C / 20°C	Measurement	18.3°C	8.4°C
	Simulation	18.1°C	8.5°C
10°C / 20°C	Measurement	19.9°C	14.0°C
	Simulation	19.5°C	14.1°C

These surface temperature differences in the SA/nSA absorber are probably due to the idealization of a double glass unit with TIM on a homogenous volume, as well as an impact of material characteristics on a temperature gradient. The total heat flux q [W/m²] by conduction and form radiation in the SA/nSA absorber is compared in Table 4. The radiation heat flux from the surface of the selective absorber ($\varepsilon = 0.06$) is simulated in the range of $q_{rad} = 0.60$ W/m² to $q_{rad} = 5.90$ W/m². On the other hand, the radiation heat flux from the surface of non-selective absorber ($\varepsilon = 0.94$) is obtained in the range of $q_{rad} = 31.9$ W/m² to $q_{rad} = 126.9$ W/m² (Table 4).

As a result, the radiation heat flux from the SA/nSA absorber, the temperature difference in airspace located between a double glass unit with TIM and the SA/nSA absorber are induced (Figure 7).

Table 4 Heat fluxes in selective/non-selective absorber

Temperature Gradient	Heat Transfer	SA	nSA
-20°C / 20°C	Conduction	17.4 W/m²	6.60 W/m²
	Radiation	5.90 W/m²	126.9 W/m²
-10°C / 20°C	Conduction	13.3 W/m²	5.40 W/m²
	Radiation	3.60 W/m²	94.1 W/m²
0°C / 20°C	Conduction	9.50 W/m²	4.00 W/m²
	Radiation	1.90 W/m²	63.7 W/m²
10°C / 20°C	Conduction	5.20 W/m²	2.20 W/m²
	Radiation	0.60 W/m²	31.9 W/m²

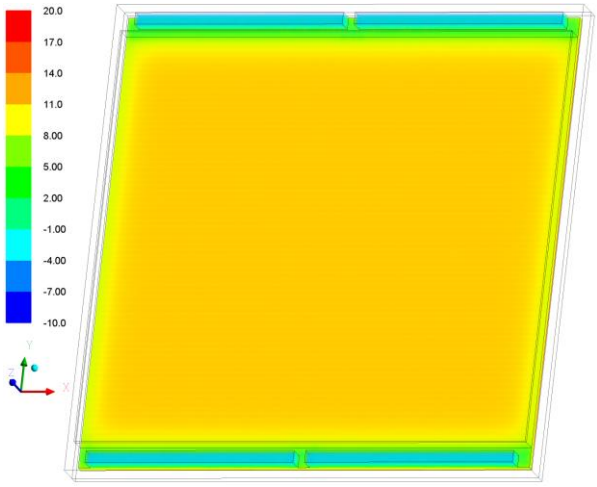

Figure 7 – Air temperature in air space of selective absorber for temperature gradient -10°C / +20°C.

Finally, it results in a temperature difference in the range of 1.84 to 9.93°C for the SA and a range of 1.92 to 11.1°C for the nSA absorber. Physically, the surface temperature difference in airspace causes airflows in its space (Figure 8). These airflows in the air space increase convection heat transfer between the SA/nSA absorber and the double-glass unit with TIM. This leads to heat transfer by convection depending on the temperature difference and, thus, a higher temperature gradient in the

airspace induces a lower thermal resistance of the studied TIF (Table 5).

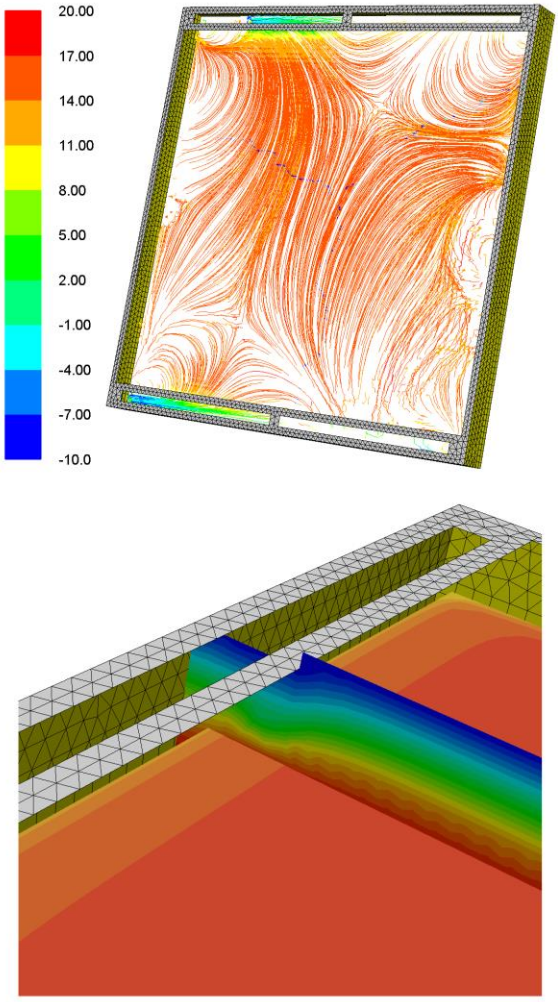

Figure 8 – Airflows and air temperature in air space with SA for temperature gradient -10°C / +20°C.

Table 5 Simulated thermal resistance

Temperature difference (K)	Simulated thermal resistance R_{sim} (m²·K)/W	
	SA	nSA
10	1.70	1.23
20	1.65	1.24
30	1.61	1.25
40	1.55	1.25

Convective heat transfer approximation

Theoretical results are compared with experimental measurement to demonstrate the consistency between all methods involved. Based on results obtained, a convective heat transfer approximation is provided.

Overall, the thermal resistance of the studied transparent insulation façade (TIF) in Table 6 is strongly dependent on the temperature gradient, especially for the selective absorber model, and these aspects show a significant difference between the selective and the non-selective absorber. It results in difference of thermal resistance up to 11% in the case of a selective absorber and about 3% in the case of a non-selective type, both for the measured R_{meas} and simulated R_{sim} values. On contrary the standard calculation results indicate slightly different thermal resistance values R_{calc} that are mostly overestimated. The higher the temeprature gradient of SA model is, higher the difference of thermal resistance between measured and claculated values obtained.

As a result of this fact, a temperature gradient effect on convective heat transfer can be aproximated according to standardized emprical relation (3). Thus, a new exponentiation value is derived and introduced to approximate calculated results with measurement (5). Instead of temperature gradient exponentiation at value 1/3 (see Eq. 3), the value of 2/5 is used. This applies for unvented airspace with low-e functionality and when the temperature difference across the airspace exceeds 5 K.

$$h_{a\_aprox} = 0.73 \times \Delta T^{2/5} \quad (5)$$

Based on calculated results R_{aprox} using new convective heat transfer aproximation (Table 6), in this way, there can be seen a good consistency between measured and newly calculated values.

Table 6 Comparison of thermal resistance R [m².K/W]

Temperature Gradient		R_{meas}	R_{sim}	R_{calc}	R_{aprox}
-20°C / 20°C	SA	R = 1.55	R = 1.55	R = 1.64	R = 1.58
	nSA	R = 1.23	R = 1.25	R = 1.33	R = 1.32
-10°C / 20°C	SA	R = 1.62	R = 1.61	R = 1.68	R = 1.62
	nSA	R = 1.24	R = 1.25	R = 1.33	R = 1.32
0°C / 20°C	SA	R = 1.67	R = 1.65	R = 1.73	R = 1.67
	nSA	R = 1.23	R = 1.24	R = 1.32	R = 1.32
10°C / 20°C	SA	R = 1.73	R = 1.70	R = 1.76	R = 1.76
	nSA	R = 1.22	R = 1.23	R = 1.31	R = 1.31

CONCLUSION

A comparative investigation of the thermal performance of a transparent insulation façade (TIF) was conducted using both experimental and theoretical methods. The experimental climatic chamber, standard calculation and CFD simulation results were compared for it to provide a degree of consistency between the theoretical results

and the experimental data. The results obtained through this approach are expected to provide a thermal characterisation of a TIF system for building energy simulation modelling of TIM based opaque building elements. Presented study demonstrated that modelling of analysed TIM glazing unit on a solid volume level was an adequate manner for its performance prediction evaluation. This will lead over further use of the numerical model to explore the thermal characteristics of a transparent insulation system incorporated in solar façade under different boundary conditions and further façade optimization studies. The effects of wind and solar radiation are also needed to study in future models.

NOMENCLATURE

Symbol	Expression	Unit
θ	Temperature	[°C]
h_a	Convective heat transfer	[W/(m^2.K)]
h_r	Radiative heat transfer	[W/(m^2.K)]
q	Heat flux	[W]
R	Thermal resistance coefficient	[m^2.K/W]
T	Thermodynamic temperature	[K]
Greek symbols		
ε	Emissivity	[-]
ρ	Reflectance	[-]
σ	Stefan–Boltzmann constant	[-]
Δ	Gradient	[-]
Subscripts		
a	Convection and conduction	
ai	Indoor air	
ae	Outdoor air	
DG	Double glazing	
DO	Discrete ordinates	
g	Air space	
GHB	Guarded hot box	
HFP	Heat flow plates	
LW	Longwave radiation region	
r, rad	Radiation	
si	Surface internal	
se	Surface external	
SA	Selective absorber type	
nSA	Non-selective absorber type	
TIM	Transparent insulation material	
TIF	Transparent insulation façade	

ACKNOWLEDGMENT

This research is supported by the project GA 16-02430Y of Czech Science Foundation, the project No. LO1408 "AdMaS UP – Advanced Materials, Structures and Technologies", supported by Ministry of Education, Youth and Sports under the "National Sustainability Programme I" and VEGA No. 1/0945/16 research project of University of Žilina.

REFERENCES

Avedissian, T., Naylor, D., 2008. Free convective heat transfer in an enclosure with an internal louvered blind International, J. Heat Mass Transf. 51, 283–293.

Brandl, D., Mach, T., Kaltenecker, P., Sterrer, R., Neururer, C., Treberspurg, M., Hochenauer, C., 2015. CFD assessment of a solar honeycomb (SHC) façade element with integrated PV cells. Sol. Energy 118, 155–174.

Brandl, D., Mach, T., Hochenauer, C., 2016. Analysis of the transient thermal behaviour of a solar honeycomb (SHC) façade element with and without integrated PV cells. Sol. Energy 123, 1–16.

Gan, G., 2001. Thermal transmittance of multiple glazing: computational fluid dynamics prediction, Appl. Therm. Eng. 21, 1583–1592.

ISO. 2007. ISO 6946:2007, Building components and building elements -- Thermal resistance and thermal transmittance -- Calculation method. Geneva, Switzerland: International Organization for Standardization

Sun, Y., Wu Y., Wilson, R., Lu, S., 2016. Experimental measurement and numerical simulation of the thermal performance of a double glazing system with an interstitial Venetian blind, Build. Environment 103, 111–122.

Sun, Y., 2017. Glazing system with transparent insulation material for building energy saving and daylight comfort. PhD thesis, Faculty of Engineering, University of Nottingham, p. 201.

Sun, Y. Liang, R., Wu, Y., Wilson, R., Rutheford, P., 2017. Development of a comprehensive method to analyse glazing systems with Parallel Slat Transparent Insulation material (PS-TIM), Appl.Energy 205, 951–963.

Sun, Y. Liang, R., Wu, Y., Wilson, R., Rutheford, P., 2018. Glazing systems with Parallel Slats Transparent Insulation Material (PS-TIM): Evaluation of building energy and daylight performance Energy Build., 159, 213–227.

Software ANSYS version 17.2, Academic research licence at Brno University of Technology, User Guide online, [URL: http://www.ansys.com]